



American Society of
Mechanical Engineers

ASME Accepted Manuscript Repository

Institutional Repository Cover Sheet

Hossein
Serhiy

Balaghi Enalou
Bozhko

First

Last

ASME Paper Title: Electric Power Transfer Concept for Enhanced Performance of the More Electric Engine

Authors: Hossein Balaghi Enalou, Serhiy Bozhko

ASME Journal Title: Journal of Engineering for Gas Turbines and Power

Volume/Issue _143 (9) Date of Publication (VOR* Online) April 19,
2021

ASME Digital Collection URL: <https://asmedigitalcollection.asme.org/gasturbinespower/article/143/9/091002/1098>
Power-Transfer-Concept-for-Enhanced

DOI: <https://doi.org/10.1115/1.4050154>

*VOR (version of record)



Electric Power Transfer Concept for Enhanced Performance of the More Electric Engine

Hossein Balaghi Enalou, and Serhiy Bozhko

University of Nottingham, Nottingham, NG7 2TU, UK

In future electrified aircraft, multi-spool more electric engines (MEEs) are expected to be equipped with electric generators connected to each shaft for power offtake and supplying onboard electrical loads. These can be interfaced to a common high-voltage DC bus architecture via power electronic converters. Such system architecture enables the establishment of an "electrical bridge" to circulate the desired amount of power between the engine shafts, and decouple their speeds. This paper introduces the possible benefits from the Electric Power Transfer (EPT) for engine performance and scrutinizes a novel EPT-Adopted Design (EPTAD) for future MEEs. For this purpose, a 0-dimensional engine model has been developed by using the inter-component-volume (ICV) method. By using the engine model, the CFM56-3 engine is redesigned to realize the EPTAD. Comparing the simulation results for the EPTAD and baseline CFM56-3 engines shows significant improvement for engine performance in terms of SFC and surge margin, mainly at cruise condition. Results show that almost 3.2% and 2.2% of fuel burn reduction is achieved for the short- and medium-haul flights respectively, with a 1150 kW EPT system. It is also shown that Variable Bleed Valves (VBVs) can be eliminated in the EPTAD engine with a 1150 kW EPT system.

Keywords: More Electric Engine (MEE), Electric Power Transfer (EPT), Variable Bleed Valves (VBVs)

I. Nomenclature

0-D	zero dimensional
AC	alternating current
APU	auxiliary power unit
BPR	bypass ratio
CC	combustion chamber
CN	non-dimensional corrected speed
CR	cruise
CW	corrected flow (kg/s)
DC	direct current
ECS	environmental control system
ED	energy density (kJ/kg)
END RWY	end of runway
EPT	electric power transfer
EPTAD	electric power transfer adopted design
FC	fuel consumption (kg)
G	generator
HP	high pressure
HPC	high pressure compressor
HPT	high-pressure turbine
ICV	inter component volume
ISA	international standard atmosphere
LP	low pressure
LPC	low pressure compressor
LPT	low-pressure turbine
M	motor
MEA	more electric aircraft
MEE	more electric engine
MTO	maximum take-off
MTOW	maximum take-off weight
OPR	overall pressure ratio
PD	power density (kW/kg)
PO	power offtake
PR	pressure ratio
PSR	power split ratio
RMS	root mean square
S/G	starter/generator
SFC	specific fuel consumption (kg/N/s)
SLS	sea level static
SM	surge margin
SOA	state-of-the-art
TET	turbine entry temperature (K)
TOC	top of climb
VBVs	variable bleed valves
VSVs	variable stator vanes
J	shaft inertia (kg.m ²)
\dot{m}	mass flow rate (kg/s)
P	total pressure (kPa)
R	specific gas constant (J/kg/K)
T	total temperature (K)
t	time (s)
V	volume (m ³)
\dot{W}	power (Watts)

ω	speed (rad.s ⁻¹)
η	efficiency

Subscripts

24	station at HPC inlet
30	station at HPC outlet
BLD	bleed
cool-sys	cooling system
EPS	electrical power system
gen	generator
EHP	HP shaft electrical motor
ELP	LP shaft electrical motor
mech	mechanical
mot	motor
PE	power electronics
t	turbomachine

II. Introduction

Jet engines must perform well in two quite different flight regimes: low altitude and flight speed to land and take off and high altitude and high subsonic speeds to cruise efficiently. Three to four times more power is needed at take-off than at cruise. Unlike 1950s-era engines for the Boeing 707 that were sized by take-off power requirements, modern airliner engines are optimized for minimum FC at cruise but sized for power at the TOC [1].

The engine components on the LP spool are coupled to the components on the HP spool thermodynamically so that the shaft speed variations bind to each other from idle to the full power setting. The thermodynamic coupling, which causes the inevitable inflexibility of shaft speeds at the off-design condition, leads to mismatches in the performance of the compressors. These mismatches enforce the implementation of handling bleeds between the LPC and HPC to regulate the flow and to avoid surge phenomenon in the compressors. Consequently, the engine operates in

a sub-optimal condition during low-speed settings at flight phases, such as taxiing and descent. Handling bleeds diverts some of the core airflow to the bypass duct of the engine; making the engine fuel-inefficient and also causing inconsistent thrust with the flight mission at low-speed settings. In this case, any solution which can help to decouple the shaft speeds is highly desirable. Prior control schemes of the MEE elaborated on multi-spool power extraction and attempted to optimize engine performance by splitting the high-power demand of the MEA on the two spools [2-5]. To further optimize and enhance engine performance and decouple the shaft speed, this study proposes the establishment of an inter-shaft power transfer using an electrical route, i.e. electric power transfer (EPT) in the MEE. EPT is realized by the electrical machines mounted on both the HP and LP shafts, which are, by their nature, bi-directional in terms of power flow. Power transfer from the HP to LP shaft (negative EPT) can allow designers to upgrade component efficiencies by surpassing the excessive safe margins at cruise while reviving it for take-off. On the other hand, power transfer from the LP to the HP shaft (positive EPT) can improve the engine operation both in terms of fuel efficiency and SM.

Power transfer fruition goes back to the 1960s when Turunen and Collman [6] applied controlled power transfer for a regenerative/recuperative engine through a hydro-mechanical system. The engine was the General Motors Research GT-309 gas turbine operating with a free power turbine. As opposed to variable nozzle, power transfer maintained high TET at off-design conditions through adjusting the airflow to keep a relatively flat power-SFC loop, as described in [6]. However, maintaining a peak temperature does not necessarily increase the turbofan's efficiency, which depends on the flight maneuver and the direction and amount of EPT. Previous power transfer ideas such as hydro-mechanical systems have never come into practice for turbofans due to their low efficiency and complexity.

EPT systems are heavy but could be part of the AC power generation system. Remarkably, an electric bridge can be created, as shown in Fig. 1, to circulate power between the shafts, independent of their speed, with the electrical machines mounted on each of the HP and LP shafts.

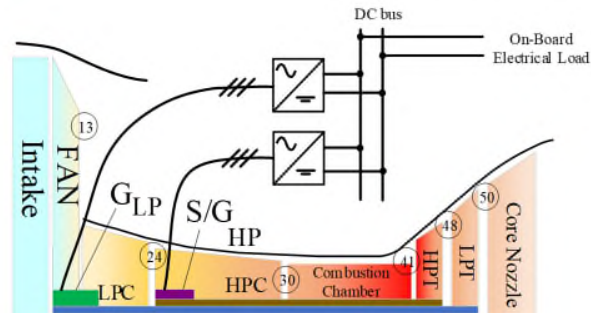


Fig. 1 Schematic diagram of a 2-spool, high bypass turbofan

EPT can be considered as a stepping-stone between the current engine architecture and disruptive innovations such as hybrid propulsion. It is also a concept that complements the hybrid propulsion concept by increasing the performance of the gas turbine since it acts as a generator. Beyond aerospace engineering, it can be applied to other applications of gas turbine engines such as the energy industry or for marine propulsion. EPT can give noticeable benefits in SFC at low-power conditions. However, at high-power settings, an ideal simple-cycle thermal efficiency is independent of TET and, as component efficiencies are starting to exceed 90%, power transfer does not give significant SFC benefit. Additionally, power transfer losses could increase SFC in real terms. Secondly, during cruise climb, which all aircraft perform to some extent, the engine operates at the cruise design condition, which is non-dimensionally optimal. As a result, power transfer cannot provide noticeable benefits for the baseline engine at cruise condition. Thirdly, any potential SFC benefit depends on the component characteristics and how they interact. One engine type may give some small benefit, typically at low power, while another may not due to different

component characteristics and the way they match. In this case, the small benefits could even turn into a loss.

The literature review reveals that EPT is still at an early stage as an innovative method for improving engine performance. Mostly, this technology has been discussed in patents rather than by research work with computational and experimental studies. Besides, no experiments have been developed to assess power transfer for the turbofans. This issue motivates the development of the present study to investigate the impact of EPT on the performance of a turbofan engine.

Possible achievements from EPT for the existing turbofans are studied by the authors of this paper in [7, 8] where it is shown that EPT does not significantly improve the baseline engine performance at high power settings [7]. The sizing point for a modern engine is now at the TOC rather than at take-off as it was in the past century. One result of these factors is that the take-off, climb, and cruise throttle settings are not very different on a modern engine. Relative to an automotive internal combustion engine averaged over its driving cycle, there is relatively little engine efficiency to be gained over an airliner mission from power transfer to optimize its cycle since current aircraft gas turbine engines are already optimized for maximum cruise efficiency where most of the fuel is consumed [1].

In order to further utilize the EPT system, mainly for high power settings such as cruise, this study suggests a novel redesign of the engine with an integrated EPT system. The novel integrated design is expected to manipulate the engine operational limits to increase the engine core pressure ratio to its maximum available value at cruise condition which was already limited for the state-of-the-art baseline engine. For this purpose, a zero-dimensional (0-D) model for a CFM56-3 engine is used which has been developed by using the well-established inter-component-volume (ICV) method and validated by comparing the simulation results with the field test data from the CFM56-

3 engine [7]. In this paper a detailed study of the performance of the novel configuration is presented and the overall impact of EPT on the future MEE is assessed by evaluating the EPT system's weight penalty.

III. Engine modeling

The ICV method [7] is used to model the engine's behavior. In the ICV method, the engine components have their own distributed gas volume storage, causing a lag in flow transfer. The mass storage capacity of the engine is assumed to be concentrated between the engine components (shown in Fig. 2). This means that some allowance should be made for the volume of the adjacent components in deciding a value for the ICVs [9]. The engine model includes component, ICV, inertia, and combustor modules. The electrical machines interact with the engine thermodynamic model through the shaft inertia modules, which use Newton's Second Law. It is important to maintain mass/momentum/energy conservation through these modules. The ICV and component modules are elaborated on in [7].

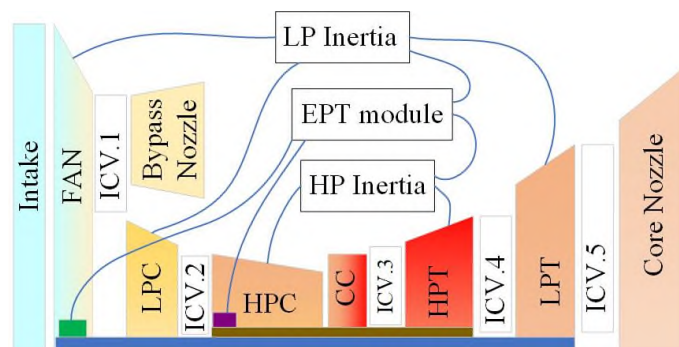


Fig. 2 ICV model structure

ICVs are dynamical subsystems within which pressures are state variables. These states are fed back and used in the previous or next component to obtain other performance variables by using thermodynamic laws and component maps. The operating points of the components are dictated

by the pressure states obtained from the surrounding ICVs. The main assumptions in the model are:

- using scaled generic component maps instead of real engine component maps;
- using the same map for various bleeding geometries at low speed settings;
- neglecting the net heat transfer between the gas path and the engine carcass.

The great advantage of the model is its modularity, which suggests its application for various engines. It contains the engine maps which are adequate for presenting the main thermodynamic behavior of the engine. The ICV method has been validated by comparing the simulation results with field test results for a three spool aero-derivative engine for both steady state and transient performance in [10] and for steady-state performance of the CFM56-3 engine in [7].

In order to study the impact of electric power transfer, the model is tailored for the CFM56-3 engine by scaling generic maps to fit the cycle design point of the CFM56-3 engine presented in Table 1. Details of the engine model for the EPT purpose is presented in [7]. Validation with the test results in [7] indicates that the steady-state errors of the simulated engine variables such as speed and SFC are less than 1% and 3.5% for the high- and low-speed settings, respectively. This suggests an acceptable level of accuracy for the electric power transfer studies.

Table 1 CFM56-3 engine reference cycle point at ISA-SLS condition

	Temperature (K)	Pressure (kPa)
Fan inlet	288	101
Fan exit	338	166
LPC exit	368	215
HPC exit	778	2405
HPT inlet	1550	2327
LPT inlet	1135	571
LPT exit	848	141
HP spool speed	14070 rpm (98%)	
LP spool speed	4739 rpm (98%)	
BPR	5.1	

IV. EPT system

Redistribution of the desired amount of power between the engine shafts, independent of their speeds, can be easily handled by using power electronic converters within the common high-voltage DC bus configuration, shown in Fig. 3. In this architecture, power electronic converters convert all of the motor/generator outputs to a high-voltage DC output, through a supervisory controller, to share the load between the sources. The DC power can then be exported to transmission systems around the airframe.

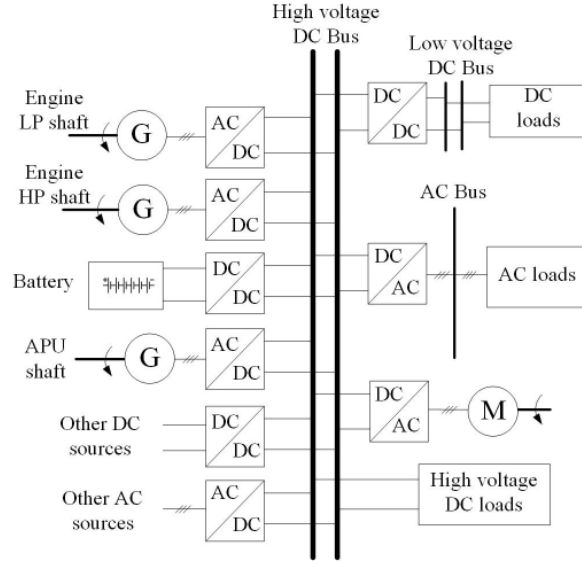


Fig. 3 High voltage DC bus architecture

In order to realize EPT in this architecture, one of the electrical machines can control the DC link voltage, while the other one can be in current control mode to manage the amount of EPT. This configuration accommodates an engine with flexible power-split-ratio (PSR) at different operational speeds depending on the amount of EPT as described with the relations below:

$$\eta_{mech,HP} \dot{W}_{HPT} - \dot{W}_{HPC} + \dot{W}_{EHP} = J_{HP} \omega_{HP} \dot{\omega}_{HP} \quad (1)$$

$$\eta_{mech,LP} \dot{W}_{LPT} - \dot{W}_{FAN} - \dot{W}_{LPC} + \dot{W}_{ELP} = J_{LP} \omega_{LP} \dot{\omega}_{LP} \quad (2)$$

$$\dot{W}_{ELP} + \dot{W}_{EHP} + \dot{W}_{EPS} + \dot{W}_{loss} = 0 \quad (3)$$

where \dot{W} , J , ω and η_{mech} stand for power, shaft inertia, speed and mechanical efficiency of the shaft, \dot{W}_{ELP} and \dot{W}_{EHP} are the shaft power of EPT motors on the LP and HP shafts, \dot{W}_{loss} is the electrical system power losses and \dot{W}_{EPS} is the onboard MEA electrical power system load on the DC bus. In this paper, analysis is conducted assuming that a constant on-board electrical load is being applied on the DC bus. Details of the application of DC bus architecture for EPT are presented in [7, 11, 12].

Continuous advancement in electrical machines power electronics allows for the design and fabrication of high power density motor drives and generation units with higher reliability and efficiency. Table 2 presents the assumptions for power or energy densities (PD/ED) and efficiencies for state-of-the-art (SOA) and future technologies in the next 10 to 15 years [13]. The main contributors to machine losses are: the iron losses which depend on frequency squared, and the copper losses which depend on the RMS current squared. Since the electrical machines have the same current and speed at motoring and generating modes, they have the same efficiency in both modes. The wire efficiency is 0.998 and its power density depends on the configuration [14]. However, in the EPT configuration, they are so short that they can be ignored.

Table 2 Technology assumptions [1, 13-15]

	PD/ED (kW/kg)		Efficiency (%)	
	SOA	Future	SOA	Future
Electric machines	13	20	95.0	96.5
Power electronics	14.3	26	97.5	98.5
Cooling system	15	20	-	-

The efficiency of the EPT system can be calculated from the efficiencies of the electrical machines, η_{mot} and η_{gen} , and power electronics, η_{PE} , as below:

$$\eta_{EPT} = \eta_{mot} \times \eta_{PE} \times \eta_{PE} \times \eta_{gen} \quad (4)$$

The EPT system mass can be calculated from the equation below:

$$Mass_{EPT} = \frac{Power_{EPT}}{PD_{mot}} + 2 \times \frac{Power_{EPT}}{PD_{PE}} + \frac{Power_{EPT}}{PD_{gen}} + \frac{(1 - \eta_{EPT}) \times Power_{EPT}}{ED_{cool-sys}} \quad (5)$$

Applying the component efficiency values from Table 2, the efficiency and mass of a 1150 kW EPT system are: 85.8% and 349 kg with the SOA technology, and 90.3% and 210 kg with the future technology, respectively.

On the other hand, the mass of the single shaft PO system of 200 kW for the MEA on-board loads is 31 kg and 19 kg with the SOA and future technologies, respectively. It can be assumed that the EPT weight overlaps by approximately 20% of the PO system weight, which results in the EPT system weight being 343 kg and 206 kg for the SOA and future technologies, respectively.

Since the electrical system dynamics are much faster than the engine dynamics, a functional model, shown in Fig. 4, is enough to study the impact of EPT on engine performance. The value of the electric power transfer, \dot{W}_{EPT} , sets the value of the HP machine shaft power, \dot{W}_{EHP} . The value of the LP machine shaft power, \dot{W}_{ELP} , is determined after consideration of the amount of on-board electrical load on the dc bus, \dot{W}_{EPS} . Positive power flow direction is defined as the power transfer from the LP to HP shaft and vice versa. A detailed EPT system model requires shaft speed as an input for the electrical machine's model, which is not in the scope of this study but has been elaborated on in [8].

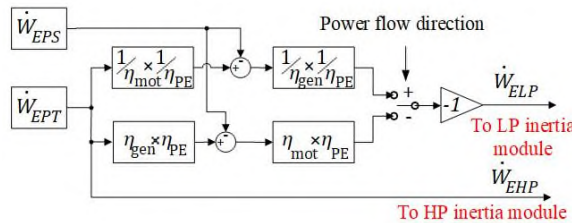


Fig. 4 EPT module block diagram

V. Electric Power Transfer Adopted Design (EPTAD)

To utilize the EPT system benefits with the privilege of independent shaft speed manipulation, a novel Electric Power Transfer Adopted Design (EPTAD) is suggested in this study. EPTAD is realized by redesigning the baseline CFM56-3 engine. The reason for selection of CFM56-3 is its available baseline performance data in the literature. Generic maps have been scaled to match the design point of the CFM56-3 engine. To utilize the maximum available core pressure ratio at cruise condition, the swallowing capacity of the LPT is higher in EPTAD to increase the PSR between the HPT and LPT from the baseline value of 56.6/43.4 to 59.5/40.5 for the EPTAD.

The PSR between the HPT and LPT is determined by the downstream pressure of the HPT, which is mainly a function of the LPT corrected massflow rate. If the design capacity (corrected massflow rate) of the LPT increases, it can accept more mass flow, which decreases HPT upstream pressure in the control volume between the HPT and LPT.

Figure 5 compares the operation points of the baseline and EPTAD engines for the same amount of thrust at cruise and MTO. For the same thrust as the baseline engine, the LPC corrected speed of the EPTAD remains approximately the same as the baseline, since the fan provides 80% of the thrust on the LP shaft. The corrected flow of the LPT map for the EPTAD engine is higher to increase the HPT pressure ratio. The HPT blades should be modified to structurally tolerate a higher pressure ratio due to the redesign of the LPT. However, the HPT map is not expected to show a noticeable change. As is shown in Fig. 5 for the EPTAD, compared to their baseline values, the HPT and LPT operate at higher and lower pressure ratio, respectively. The redesign will shift the HPC corrected speed at the cruise condition from the baseline value to maximum value for the EPTAD to reach the maximum available core pressure ratio while not violating any of the engine limits at cruise condition.

Some of the compression and expansion is shifted from the LP components to the HP components through increasing the PSR of HPT to LPT. The main target of the EPTAD engine is to keep the HPC corrected speed at its maximum allowable value for all engine operation modes. This increases the core pressure ratio which improves the overall efficiency. However, the overall efficiency can also be degraded by EPT losses and reduction in HPC and LPC efficiencies as is shown Fig. 5. In this paper, simulation results show that the fuel consumption is reduced after considering the combination of these effects.

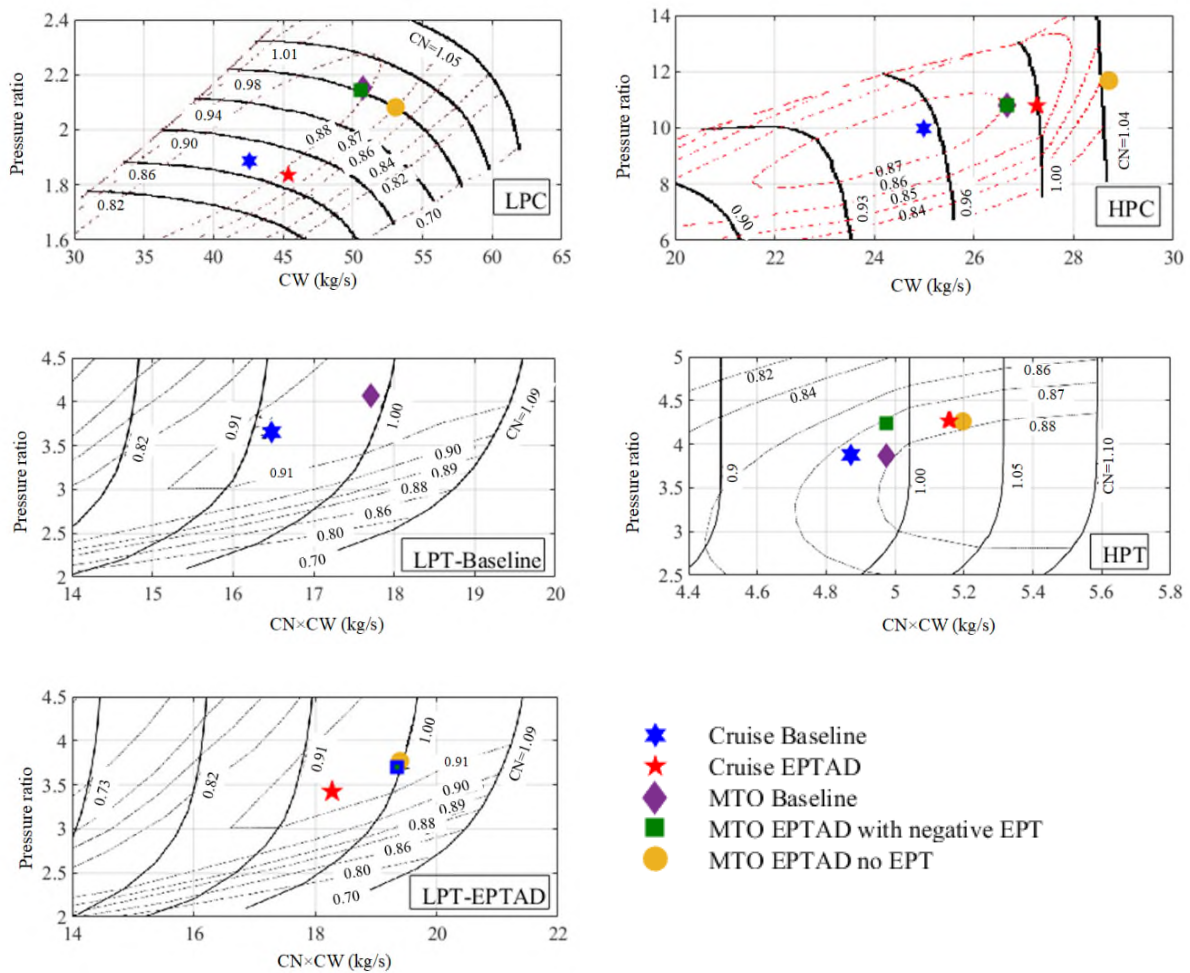


Fig. 5 Comparison of EPTAD operating points on engine maps

The redesign of the turbine section will lead to over-speed of the HP shaft during scenarios, such as MTO and TOC, where the baseline HPC corrected speed was at maximum permissible value. The over-speed can be compensated by EPT from the HP to LP shaft (negative EPT) to keep the HP speed below its permissible value for the EPTAD, assuming the LP speed is controlled by the engine controller. The direction of the required EPT for the EPTAD is presented in Table 3. At high-power settings, negative EPT is implemented to prevent HP shaft over-speed, while at low-power settings such as idle mode, positive EPT is implemented to increase the HPC corrected speed and engine efficiency. In Section VI, results show that for the redesign of the CFM56-3 engine, the maximum amount of required EPT at the high power settings is around 1 MW which is almost 5% and 26% of HP shaft power at MTO and cruise condition, respectively. The FC change by the EPTAD compared to the baseline engine is also presented in Table 3.

Table 3 EPT direction and FC change for EPTAD engines

	EPT direction	FC
Cruise	No EPT	Decreased (-)
MTO	Negative EPT	Increased (+)
END RWY	Positive EPT	Decreased (-)
TOC	Negative EPT	Increased (+)
Idle	Positive EPT	Decreased (-)

At high power settings, the matching between the LPC and HPC remains the same due to the similar compressor PSR and corrected speed of the EPTAD and baseline engines. Thus, at MTO and TOC, SMs of the HPC and LPC remain approximately the same as the baseline engine. At low-speed settings, such as idle mode, with a higher HPC corrected speed for the same baseline LPC corrected speed, the flow matching between the EPTAD compressors will change, leading to much higher LPC SM and a small increase in HPC SM. Due to the fast response of the EPT system for any disturbance in engine performance, SMs can be quickly recovered.

Moreover, the HPC corrected speed range of the EPTAD becomes narrower, which suggests optimization of the HP section including the HPC, HPT and HP generator. The design point of the HPC can move to higher corrected speeds to have maximum efficiency at maximum speed which will further increase the EPTAD efficiency. EPT may increase the LPC corrected speed variation slightly; however, the baseline LPC corrected speed changes over a wide range, which does not lead to any significant further improvements nor degradations of LP component efficiencies.

VI. Simulation Results

This section presents simulation results at high and low-speed settings to evaluate the performance of the EPTAD. The results for the impact of EPT on the baseline engine performance have been previously published in [8, 16]. In this paper, the focus is on the EPTAD studies. The model can represent the transient behavior at flight maneuvers such as go-around as well, which is the focus of future studies. In this paper, negative EPT means power flow from the HP to LP shaft and vice versa and per-unit quantities are fractions of their value at MTO. SM is also defined as below:

$$SM = 100 \times \left(\frac{PR_{surge}}{PR_{operating\ point}} - 1 \right) \quad (6)$$

where PR_{surge} is the pressure ratio of the surge line at the same operating corrected massflow rate.

A. Cruise, MTO and TOC Scenarios

For the sake of simplicity, four main points within the mission profile were chosen: MTO, end of runway (END RWY), TOC and cruise (CR), as is shown in Table 4. With these checkpoints, the performance of the engine can be assessed at take-off, climb and cruise. These four segments were considered as electrification implications have bigger impact in these segments.

Table 4 Mission profile checkpoints with flight conditions

	Mach	Altitude (m)	Net Thrust (kN)
MTO	0	0	97.4
END RWY	0.23	0	70.0
TOC	0.79	11887	30.2
CR	0.79	11887	21.9

As previously discussed in Section V, to exploit EPT at high power settings, EPTAD is proposed. In order to realize maximum HPC corrected speed with no EPT (no EPT losses), the PSR between the HPT and LPT is increased (by approximately 3%), for the same baseline LPC corrected speed. To address HP shaft over-speed at MTO, -1150 kW of EPT is required to keep the same HPC corrected speed (0.98). At the same time, the fuel controller maintains the LPC corrected speed to provide approximately the same baseline thrust as is presented in Table 5. To have a better comparison in terms of propulsive efficiency, thrust is fixed for the EPTAD and baseline engines. By keeping this constraint, in order to move the HPC corrected speed from 0.95 to 1.00 at cruise condition, LPT should be redesigned for a 9% increase in its corrected flow to increase the HPT expansion ratio adequately.

The EPTAD satisfies the operational limits of the baseline engine such as the maximum allowable TET (assumed 1550 K for the studied engine) and surge margins at MTO and TOC. However, by keeping the same HPC corrected speeds, the SFC increases in TOC and MTO and maximum available thrust decreases slightly at MTO due to the EPT losses.

At cruise, the LPC SM improves by 11.8% at cruise condition due to higher HPC corrected speed, and the HPC SM is slightly higher than its baseline values. EPTAD reduces the baseline SFC by 1.67% for the cruise condition which also decreases TET due to lower fuel rate at higher core air flow. The corrected shaft speeds are the same at their maximum value where EPTAD requires -306 and -1150 kW of EPT at TOC and MTO, respectively.

Table 5 Baseline and EPTAD performance at cruise, MTO and TOC

	Cruise		MTO		TOC	
	Baseline	EPTAD	Baseline	EPTAD	Baseline	EPTAD
EPT (kW)	0	0	0	-1150 kW	0	-306
Thrust (kN)	21.9	21.9	97.4	96.5	30.2	30.2
HP CN	0.95	1.00	0.98	0.98	1.00	1.00
LP CN	0.88	0.88	0.98	0.98	1.00	1.00
OPR	18.9	19.1	23.3	23.1	24.4	24.5
TET (K)	1234	1200	1550	1550	1358	1360
SFC change (%)	-	-1.7	-	+0.4	-	+0.5
LPC SM (%)	21.9	33.7	29.8	29.1	32.5	33.6
HPC SM (%)	22.4	22.8	19.2	19.1	18.3	18.5

The cruise condition in Table 5 is a single point. The thrust during cruise varies, therefore the SFC should be analyzed over a thrust range rather than at a single point. The thrust range for a typical flight at different altitudes and Mach numbers is shown in Table 6. As is shown in Fig. 6, the average SFC change of the EPTAD compared to the baseline engine is approximately 1.6%. Figure 7 shows if the EPTAD is designed for a cruise design point, EPT is required to keep the HPC corrected speed at 1.00 for other cruise conditions with different thrust values.

Table 6 Cruise thrust at different altitudes and Mach numbers

Alt (m)	Mach number	Thrust (kN)
11277.6	0.79	23.6
11887.2	0.79	22.7
11887.2	0.79	21.9
12496.8	0.79	21.0
12496.8	0.79	20.2
12496.8	0.79	19.5

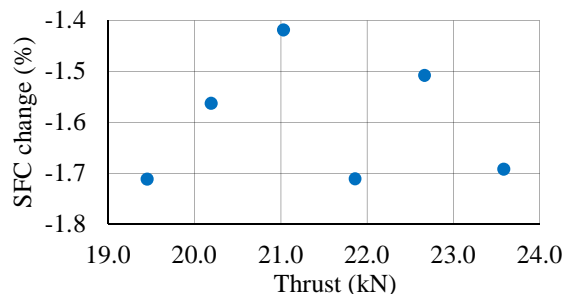


Fig. 6 SFC change at cruise at different thrust values

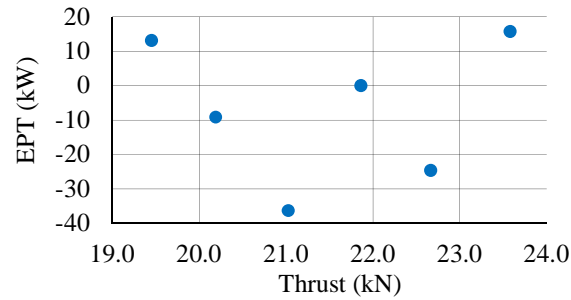


Fig. 7 EPT values at cruise at different thrust values

As discussed before, negative EPT is implemented to avoid over-speed of the HP shaft at high speed settings such as MTO and TOC. Figure 8 shows that the compressors will not surge if the EPT system fails. In simulation, the required EPT has been set to zero by a step change to investigate the transient impact. The operating points on the LPC move away from the surge line and the operating points of the HPC move to higher corrected speeds while not violating surge margin significantly. The HPC corrected speed should decrease back to lower values by decreasing the engine throttle if the EPT system fails.

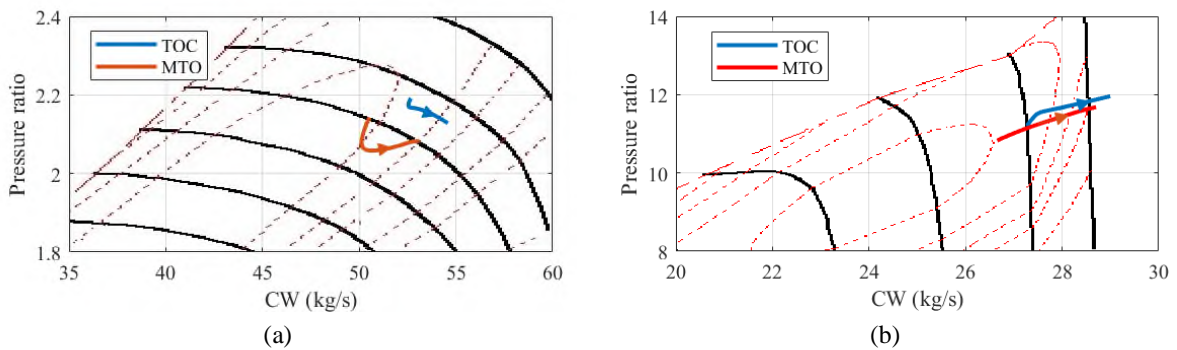


Fig. 8 Operating lines of compressors at TOC and MTO with EPT failure, a) LPC map, b) HPC map

B. Climb Scenario

For climb manoeuvre, the thrust settings from END RWY up to TOC are implemented from Table 4, assuming a linear thrust and Mach number change based on the altitude. As is shown in Fig. 9, TET is decreased at initial phase of climb, since the SFC is lower and the core airflow is higher

with higher HPC corrected speed in EPTAD compared to the baseline value (see Fig. 10). At TOC, the HPC corrected speed is kept the same as the baseline engine with the EPT losses, which increases SFC and TET as shown in Fig. 11 and Fig. 9. The SFC decreases at the initial phases of climb due to higher core pressure ratio, while the benefit is cancelled out at higher altitudes up to TOC due to the EPT losses. The overall FC during climb depends on the amount of required thrust. As is shown in Fig. 12, the amount of EPT is positive at initial phase of climb to move the HPC corrected speed to 1.00, while it becomes negative beyond approximately 1.5 km to keep the HPC corrected speed at 1.00.

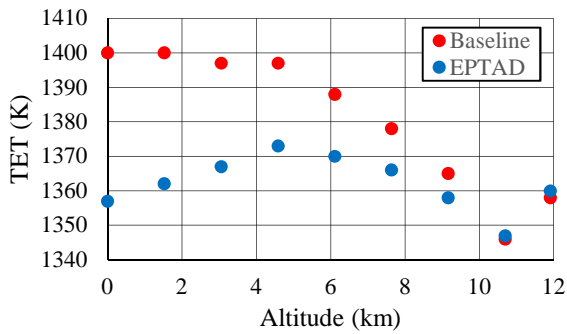


Fig. 9 TET (END RWY to TOC)

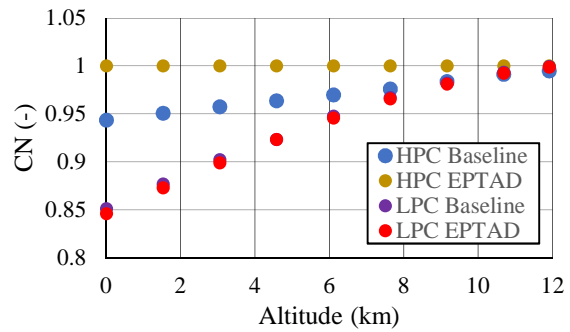


Fig. 10 Corrected speeds (END RWY to TOC)

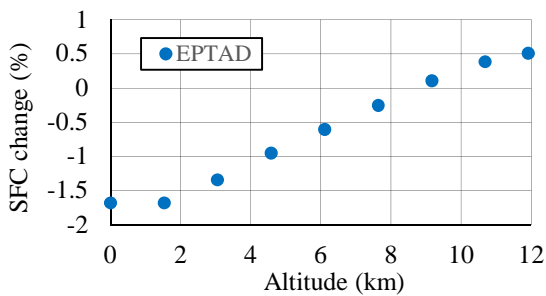


Fig. 11 SFC (END RWY to TOC)

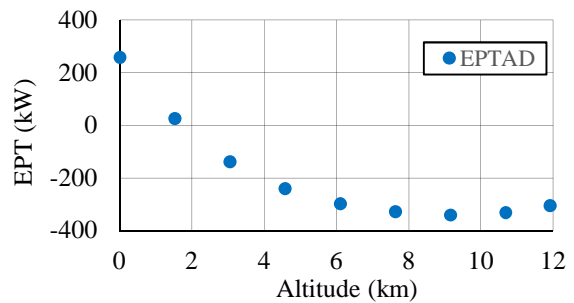


Fig. 12 EPT (END RWY to TOC)

C. Bleeding Removal

Due to unavailability of compressor maps for inter-stage VBVs, their impact is not considered in the model, while the downstream VBVs module is modelled as an open-loop reduction in mass

flow, scheduled against LPC corrected speed. The extracted bleeding flow from the downstream ICV of the LPC VBV is fed to the ICV of the duct. If the HPC corrected speed is appropriately matched with the LPC corrected speed at low-speed settings, there will be no need for air bleeding. By positive EPT at low speed settings, the HPC corrected speed increases considerably which suggests decrease or removal of the air bleedings, depending on the amount of EPT. In equation (7) for the determined value of \dot{m}_{BLD} , P_{24} changes up to a point to have equilibrium point in the ICV between the HPC and LPC.

$$\frac{dP_{24}}{dt} = \frac{RT_{24}}{V_{ICV,2}} (\dot{m}_{LPC} - \dot{m}_{HPC} - \dot{m}_{BLD}) \quad (7)$$

where \dot{m}_{BLD} is the bleeding flow rate between the LPC and HPC. V_{ICV} is the constant volume of the ICV, R is the gas constant, and P and T are the outlet total pressure and temperature, respectively. The VBV is removed for the EPTAD due to different compressor matching compared to the baseline engine. The operating line on compressor maps is shown in Fig. 13. The baseline LPC SM is not violated by the removal of the VBV. As is shown in Fig. 14, at maximum HPC corrected speed, negative EPT has been implemented to avoid the HP speed exceeding its maximum permissible value. At low-speed settings, positive EPT has been implemented to increase the HPC corrected speed to move the HPC operating points to a higher corrected mass flow. The HPC map in this study is a composite compressor map with an embedded VSVs-schedule. Higher HPC corrected speed at low-speed settings also suggests the modification of VSVs, which has not been modelled in this study due to a lack of data regarding starting strategies and map changes with VSVs.

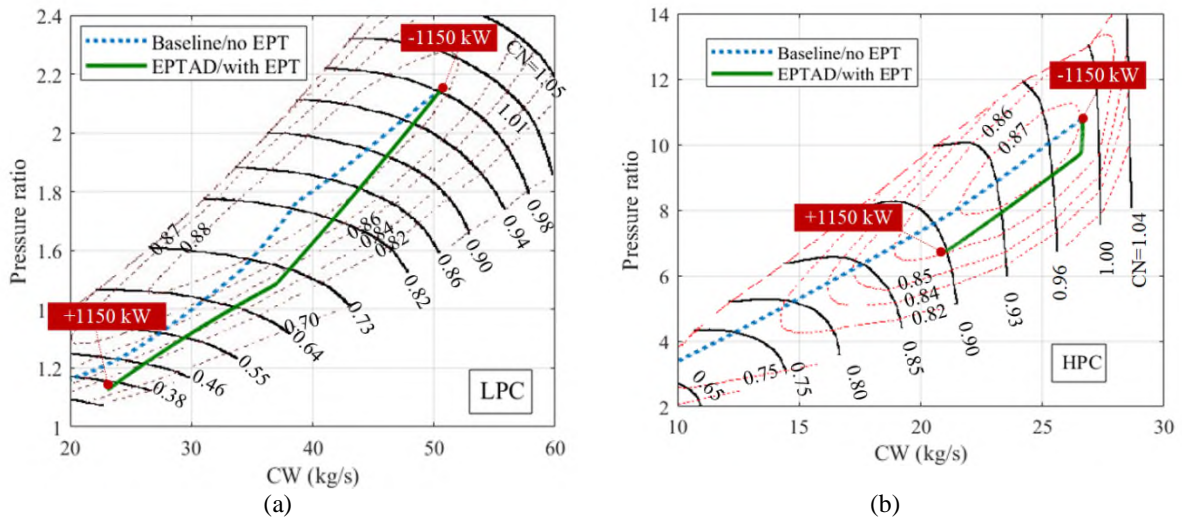


Fig. 13 LPC and HPC steady-state operating lines at ISA-SLS, a) LPC map, b) HPC map

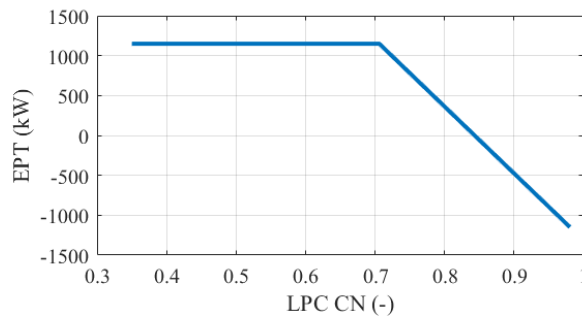


Fig. 14 Required EPT for maximum HPC corrected speed

During the descent phase, flight idle mode is selected where the engine needs to operate at a high enough power to keep the bleeding pressure higher than a minimum for its application in the ECS. The P_{30} limit controller protects against the supply pressure for ECS, which is set 250 kPa in this study. Results for flight idle, at 9 km altitude with a Mach number of 0.6, are presented. Table 7 shows that by positive EPT (+200 kW), the HPC corrected speed increases to provide a pressure of 250 kPa by the HPC. The fuel rate is decreased by 1.2 kg/min for the EPTAD, for which burner loading should be investigated in detail. For EPT over +250 kW the model is not valid due to a lack of sub-idle performance data. The decrease in fuel flow rate is because of higher HPC corrected speed which is more efficient for producing the required pressure for the ECS usage.

SMs are also higher than their baseline values due to positive EPT for the baseline and EPTAD engines. Bleed values in Table 7 and Table 8 are the percentages of bleed flow to the core flow.

Table 7 Comparison between baseline and EPTAD at P_{30} idle

	Baseline	EPTAD
P_{30} (kPa)	250	250
EPT (kW)	0	+200
Bleed (%)	42	0
HPC CN	0.81	0.84
LPC CN	0.51	0.41
Fuel rate (kg/min)	4.53	3.33
LPC SM (%)	7	15
HPC SM (%)	24	36

During flight idle, a minimum HPC corrected speed controller is activated to keep the engine ignition with an adequate core massflow rate and SMs. The baseline and EPTAD engine performance is compared by holding the HPC corrected speed at its baseline constant value (0.80) with the speed controller at 1.5 km altitude at Mach=0.4. As presented in Table 8, by adding +450 kW of EPT, the LPC corrected speed of EPTAD drops by 28%, which decreases the excessive thrust. It should be noted that lower LP rotational speed at flight idle may increase the drag and lower the thrust during descent. This might lead to a steeper descent and longer cruise, which increases FC during the end of the flight. However, most aircraft are very good gliders, so in practice the thrust is almost zero and the setting is just to maintain the engine idle speed.

Table 8 Comparison between baseline and EPTAD at flight idle

	Baseline	EPTAD
EPT (kW)	0	+450
Bleed (%)	42	0
HPC CN	0.80	0.80
LPC CN	0.46	0.33
Fuel rate (kg/min)	10.80	7.18
LPC SM (%)	7	12
HPC SM (%)	24	36

The fuel rate experiences a significant decrease by more than 30% (3.6 kg/min), and the compressor SMs also increase noticeably due to positive EPT. Assuming a linear descent, the average FC changes from Table 7 and Table 8 is -2.4 kg/min for the descent scenario.

D. Trade Study

The EPTAD engine requires a 1150 kW EPT system to enable maximum HPC corrected speed with no EPT at cruise condition. However, the 1150 kW motors are much larger than what would be typically required to generate power for a single aisle class airplane. In general, the full 1150 kW EPT system on board the airplane is required to utilize the full capacity of EPT system and removal of VBVs. In order to have a better understanding of the impact of EPT power rating on the adopted engine performance, the results with a 500 kW EPT system are presented in this section.

In order to decrease the amount of EPT, a trade-off can be considered by moving the HPC corrected speed at cruise from 0.95 to 0.97 by shifting the turbines PSR, but further increasing it to 1.00 by positive EPT. This design requires -500 kW of EPT at MTO to address HP shaft over-speed. As is shown in Table 9, +124 kW is required to increase the HPC corrected speed to 1.00 at cruise condition, which decreases the SFC by 0.64% and increase the LPC SM by 11.5% with a -26 K decrease in TET.

Table 9 EPTAD-500 performance

	cruise	MTO	TOC
EPT (kW)	+124	-500	-125
Thrust (kN)	21.9	96.9	30.2
HPC CN	1.00	0.98	1.00
LPC CN	0.88	0.98	1.00
TET (K)	1203	1550	1357
OPR	19.8	23.1	24.5
SFC change (%)	-0.64	+0.17	+0.11
LPC SM change (%)	33.8	29.1	33.6
HPC SM change (%)	22.7	19.2	18.7

By changing the turbine PSR by almost 1.5%, the HPC corrected speed at cruise point increases by 2% with no EPT and exceeds 1.00 beyond +124 kW of EPT as shown in Fig. 15.

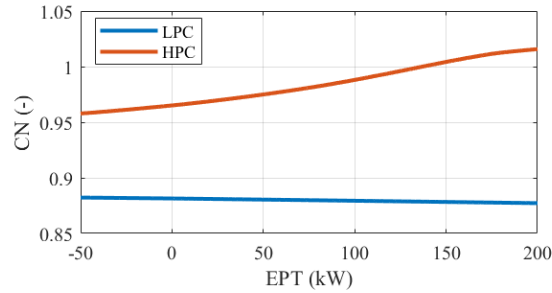


Fig. 15 Corrected speed change vs EPT for EPTAD-500

In order to consider the efficiency of all components, turbomachine efficiency is defined as the amount of power which is used to increase the pressure ratio in the compressors by the amount of power that can be extracted from the turbines. In fact, turbomachine efficiency is a metric that looks at the turbomachinery losses, power split ratio between the components and the total available power of the turbines. In this aspect, not only the components' efficiency but also their power split ratios (PSRs) play important roles for turbomachine efficiency [7]. PSR can be defined as follows:

$$PSR_{Component} = \frac{Component\ power}{Available\ Engine\ Power} \quad (8)$$

Available engine power is the total amount of power produced by the turbines. The turbomachine efficiency, η_t , can be calculated as:

$$\eta_t = \frac{-(PSR \times \eta)_{Compressor}}{(PSR/\eta)_{Turbine}} \quad (9)$$

Figure 16 depicts SFC change due to the change of η_t for various EPT values. The turbomachine efficiency declines beyond 150 kW of EPT due to fact that the EPT losses and the HPC efficiency

drop exceed the efficiency gain at higher PSR of the HPC. However, EPT is not allowed to exceed +124 kW to avoid HP over-speed.

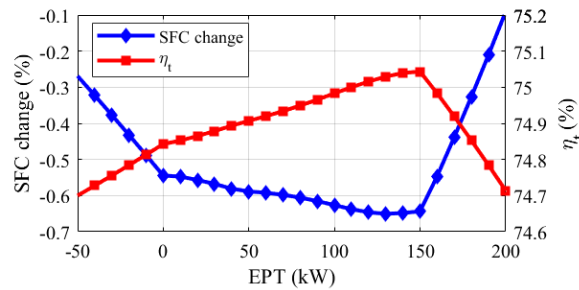


Fig. 16 Cruise SFC change and efficiency for the EPTAD-500

VBVs' opening depends on the increase of HPC corrected speed by the EPT, which is studied in detail for the baseline engine in [7]. Results in Fig. 17 show that for the baseline and EPTAD-500 with +500 kW of EPT, bleeding can be halved, and VBVs can be removed with +1150 kW of EPT for the EPTAD-1150. It should be acknowledged that the VBVs also have uses beyond lowering the stationary operating line (e. g. starting, stabilization after surge). Therefore, removing them entirely could be problematic.

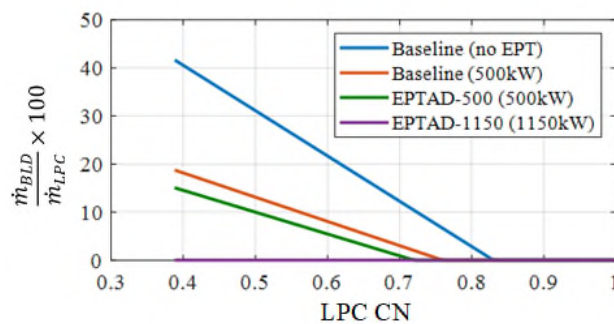


Fig. 17 VBVs re-schedule for the baseline and EPTAD engines

VII. Fuel Consumption Analysis

After studying various flight modes, including cruise and idle modes, this section investigates the differences in fuel burn due to the EPT system, and additional fuel burn due to the EPT system weight. From simulation results in Section VI, the expected average SFC change by the EPT system at various flight phases is shown in Table 10. The time of each maneuver is also obtained from [17] for a 4-hour flight.

From Section IV, the predicted mass of the proposed back-to-back 1150 kW motor generator set, including power electronics, machines and cooling system, is predicted to be 343 kg and 206 kg with the SOA and future technologies, respectively. The weight reduction due to VBV's removal, and the additional mass of the aircraft structure for extra weight at the wings is not considered in the weight analysis due to the lack of data. Moreover, at a roughly constant lift-to-drag ratio and SFC, the thrust and FC are proportional to the mass. For detailed analysis, an aircraft performance model is required to calculate the impact of weight on mission fuel burn. Considering these assumptions, the added FC due to weight of the EPT system for each engine for each flight maneuver is:

$$\text{Added FC} = \frac{\text{EPT weight}}{\text{Aircraft weight}} \times \dot{m}_{\text{fuel}} \times t \quad (10)$$

where t is the maneuver time. The maximum take-off weight (MTOW) for a B737-300 is 57,000 kg, which is reduced to almost 49,930 kg after 4 hours of flight. The values of fuel rate change and added FC are given in Table 10. They assume future EPT technologies on the B737 aircraft when fitted with two CFM56-3 engines.

Table 10 Average FC analysis for a B737 for a 4-hours flight (EPTAD-1150)

	Maneuver time	\dot{m}_{fuel} Baseline (No EPT)	\dot{m}_{fuel} change Baseline	Maximum EPT value	Aircraft weight	Added FC
Taxiing	5 min	2×9.90 kg/min	0.00 kg/min	Not studied	57000 kg	2×0.22 kg
Climb	30 min	2×32.05 kg/min	2×-0.33 kg/min	-1150 kW	56901 kg	2×4.22 kg
Cruise	175 min	2×13.33 kg/min	2×-0.21 kg/min	0 kW	54978 kg	2×10.61 kg
Descent	25 min	2×7.66 kg/min	2×-2.40 kg/min	1150 kW	50313 kg	2×0.95 kg
Taxiing	5 min	2× 9.90 kg/min	0.00 kg/min	Not studied	49930 kg	2×0.24 kg
Flight envelope	240 min	2×3584.75 kg	2×-106.65 kg	-	-	2×13.39 kg

After subtracting the added FC due to the EPT weight (2×13.39 kg), from the fuel reduction (2×-106.65 kg), up to 2.6% of fuel saving is achieved for the 4-hours flight. Table 11 presents the results for fuel saving by the EPT system with the SOA and future technologies for two flight ranges. The fuel saving is higher for short-haul flights, since the main fuel burn reduction is achieved at low-speed settings, which makes up the higher portion of the flight for short-haul flights. Table 11 also provides an insight of the penalty due to the EPT system weight. The future technologies for the EPT system are expected to decrease the FC approximately 0.4% more compared to the SOA technology.

Table 11 FC reduction by EPTAD

	4-hours flight	2-hours flight
SOA technology	$\frac{-100.7 \text{ kg} + 22.3 \text{ kg}}{3585 \text{ kg}} = -2.2\%$	$\frac{-75.9 \text{ kg} + 12.2 \text{ kg}}{1985 \text{ kg}} = -3.2\%$
Future technology	$\frac{-106.7 \text{ kg} + 13.4 \text{ kg}}{3585 \text{ kg}} = -2.6\%$	$\frac{-80.4 \text{ kg} + 7.3 \text{ kg}}{1985 \text{ kg}} = -3.7\%$

The 1150 kW motors are much larger than what would typically be required to generate power for a single aisle class airplane. In general, the full 1150 kW EPT system on board the airplane is required for the most efficient MEE at cruise condition and removal of the VBV's. On the other hand, the bulk of the benefit (from a fuel burn perspective) seems to be the reduction in thrust by

maintaining a higher HPC corrected speed during descent/approach. Therefore, it is necessary to find the optimum amount of power transfer for the EPT system design.

Figure 18 shows the results of a weight trade-off by sizing the EPT motors down to reduce the total “added” weight. Results show that for the MEE, reducing EPT power to 500 kW for both the 2- and 4-hour flights does not change the FC reduction significantly, resulting in values of almost 3.1% and 1.9%, respectively.

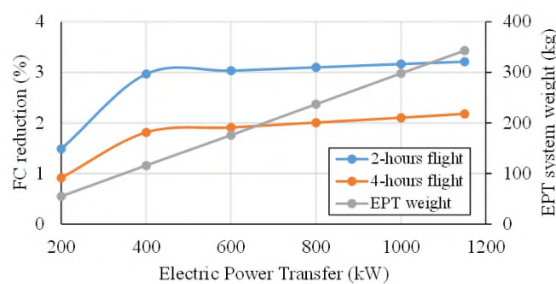


Fig. 18 FC reduction and EPT weight against EPT power

VIII. Conclusion

This paper suggests a redesign of the turbofan (EPTAD) to utilize the EPT system for high and low power settings. A 0-D engine model is developed by using the ICV method and employing performance maps and thermodynamic rules to enable turbofan performance analysis. The model suggests an acceptable level of accuracy for electric power transfer studies. Detailed simulations on the redesign of the CFM56-3 engine are performed to evaluate EPTAD performance mainly in terms of FC and SM. Results show the following.

- 1) The EPTAD moves the operation points to reach a higher overall pressure ratio which improves the MEE efficiency during the cruise, idle, and initial phase of climb, while degrading engine efficiency for TOC and MTO due to EPT losses. The EPT controller moves the HPC corrected speed to 1.00 with positive EPT when its baseline value was less

than 1.00 in maneuvers such as cruise, climb and idle, and keep it below its permissible value with negative EPT in maneuvers such as MTO and TOC.

2) VBV's can be removed by a 1150 kW EPT system and can be halved by a 500 kW EPT system. By power transfer from the LP to HP shaft, the swallowing capacity of the HPC increases so that the VBV's opening can be decreased.

3) FC with re-scheduled bleeding is decreased significantly (up to 30%) at idle scenarios with new idle set-points. MEE performance with re-scheduled bleeding, and the new idle setting, is not deteriorated in terms of surge margins. The LPC SM increases significantly (more than 5%) and the HPC SM is not degraded with the EPT system.

4) After assessing the power density of electrical machines and power electronics, it is shown that the FC for the short- and medium-haul flights reduces by up to 3.2% and 2.2% with the state-of-the-art and 3.7% and 2.6% with the future technologies with 1150 kW EPT system. System weight analysis shows that reducing the EPT power to 500 kW reduces the efficiency gains by approximately 0.2%. This suggests a more detailed trade-off analysis in future to select the optimum power.

The EPT system offers ultimate flexibility and fast control of power exchange for the future MEE. Further studies should be performed on the optimum amount of power transfer, the impact of system weight and space on propulsion efficiency, electrical system topology, electrical machines, converters etc.

IX.Acknowledgments

This project has received funding from the Clean Sky 2 Joint Undertaking under the European Union's Horizon 2020 research and innovation programme under grant agreement No 807081.

X. References

- [1] Epstein, A. H., and O'Flarity, S. M., 2019, "Considerations for Reducing Aviation's CO₂ with Aircraft Electric Propulsion," *Journal of Propulsion and Power*, 35(3), pp. 572-582.
- [2] Pluijms, A., Schmidt, K. J., Stastny, K., and Chibisov, B., "Performance Comparison of More Electric Engine Configurations," *Proc. ASME Turbo Expo 2008: Power for Land, Sea, and Air*, Paper No: GT2008-50758, pp. 50113-50122.
- [3] Speak, T. H., Sellick, R. J., Kloos, V., and Jeschke, P., 2015, "Dual Drive Booster for a Two-Spool Turbofan: Performance Effects and Mechanical Feasibility," *Journal of Engineering for Gas Turbines and Power*, 138(2), pp. 022603-022609.
- [4] Kloos, V., Speak, T. H., Sellick, R. J., and Jeschke, P., 2018, "Dual Drive Booster for a Two-Spool Turbofan: High Shaft Power Offtake Capability for MEA and Hybrid Aircraft Concepts," *Journal of Engineering for Gas Turbines and Power*, 140(12), pp. 121201-121210.
- [5] Kreuzer, S., and Niehuis, R., 2017, "Commissioning of Split Power Offtake on a Twin-Spool More Electric Engine Demonstrator," *ASME Turbo Expo 2017: Turbomachinery Technical Conference and Exposition* June 26–30, 2017 Charlotte, North Carolina, USA, p. V001T001A006.
- [6] Turunen, W. A., and Collman, J. S., 1966, "The General Motors Research GT-309 Gas Turbine Engine," *SAE Transactions*, 74, pp. 357-377.
- [7] Enalou, H. B., and Bozhko, S., 2020, "Performance Improvement of Turbofans by Electric Power Transfer," *ASME J. Turbomach*, 142(11), pp. 111002-111017.
- [8] Enalou, H. B., Le-Peuvedic, J.-M., Rashed, M., and Bozhko, S., 2018, "Potential Improvements in Turbofan's Performance by Electric Power Transfer," *SAE 2018 The Aerospace Systems and Technology Conference London Heathrow*, SAE Technical Paper 2018-01-1962.
- [9] Fawke, A. J., Saravanamuttoo, H. I. H., and Holmes, M., 1972, "Experimental Verification of a Digital Computer Simulation Method for Predicting Gas Turbine Dynamic Behaviour," *Proceedings of the Institution of Mechanical Engineers*, 186(1), pp. 323-329.
- [10] Enalou, H. B., Soreshjani, E. A., Rashed, M., Yeoh, S. S., and Bozhko, S., 2017, "A Detailed Modular Governor-Turbine Model for Multiple-Spool Gas Turbine With Scrutiny of Bleeding Effect," *J Eng Gas Turb Power*, 139(11), pp. 114501-114507.
- [11] Enalou, H. B., Lang, X., and Bozhko, M. R. S., 2020, "Time-Scaled Emulation of Electric Power Transfer in the More Electric Engine," *IEEE Transactions on Transportation Electrification*, vol. 6, no. 4, pp. 1679-1694.
- [12] Lang, X., Yang, T., Li, C., Enalou, H. B., Bozhko, S., and Wheeler, P., 2020, "A Dual-Channel Enhanced Power Generation Architecture with Back-to-back Converter for MEA Application," *IEEE Transactions on Industry Applications*, vol. 56, no. 3, pp. 3006-3019.
- [13] Sahoo, S., Zhao, X., and Kyprianidis, K., 2020, "A Review of Concepts, Benefits, and Challenges for Future Electrical Propulsion-Based Aircraft," *Aerospace*, 7(4), p. 44.

- [14] Gesell, H., Wolters, F., and Plohr, M., 2019, "System analysis of turbo-electric and hybrid-electric propulsion systems on a regional aircraft," *The Aeronautical Journal*, 123(1268), pp. 1602-1617.
- [15] Bozhko, S., Yang, T., Peurvedic, J. L., Arumugam, P., Degano, M., Rocca, A. L., Xu, Z., Rashed, M., Fernando, W., Hill, C. I., Eastwick, C., Pickering, S., Gerada, C., and Wheeler, P., 2018, "Development of Aircraft Electric Starter-Generator System Based-On Active Rectification Technology," *IEEE Transactions on Transportation Electrification*, vol. 4, no. 4, pp. 985-996.
- [16] Enalou, H. B., and Bozhko, S., 2018, "Performance Improvement of the CFM56-3 Aircraft Engine by Electric Power Transfer," 13 th European Conference on Turbomachinery Fluid dynamics & Thermodynamics April 8-12, 2018, Lausanne, Switzerland, paper ID: ETC2019-004.
- [17] Chati, Y. S., and Balakrishnan, H., 2013, "Aircraft Engine Performance Study Using Flight Data Recorder Archives," 2013 Aviation Technology, Integration, and Operations Conference, American Institute of Aeronautics and Astronautics, paper ID: AIAA 2013-4414.